C$_2$ Selectivity Enhancement in Chemical Looping Oxidative Coupling of Methane over a Mg−Mn Composite Oxygen Carrier by Li-Doping-Induced Oxygen Vacancies

Zhuo Cheng,[†,§] Deven S. Baser,[†,§] Sourabh G. Nadgouda,[†] Lang Qin,[†] Jonathan A. Fan,[‡] and Liang-Shih Fan*,[†]

[†]Department of Chemical and Biomolecular Engineering, The Ohio State University, 140 West 19th Avenue, Columbus, Ohio 43210, United States

[‡]Department of Electrical Engineering, Ginzton Laboratory, Spilker Engineering and Applied Sciences, 348 Via Pueblo Mall, Stanford University, Stanford, California 94305, United States

Ⓢ *Supporting Information*

ABSTRACT: Chemical looping oxidative coupling of methane (CLOCM) is a promising process for direct methane conversion to C$_2$ products. Under the chemical looping approach, the oxygen carrier that provides lattice oxygen, in place of molecular oxygen, is used for methane oxidation. This study performs redox experiments that probe the C$_2$ selectivity enhancement properties of a Mg−Mn composite oxygen carrier through the use of a low concentration of Li dopant. It was found that the C$_2$ selectivity of the Li-doped oxygen carrier in CLOCM is universally higher than that of the undoped Mg$_6$MnO$_8$ oxygen carrier with a maximum improvement in selectivity of ~50%. Density functional theory simulation reveals that the Li dopant has a short-range effect on the formation of oxygen vacancies. The Li-doping-induced oxygen vacancy reduces the adsorption energy of methyl radicals and increases the C−H activation barrier. These findings provide a catalytic dopant screening strategy for CLOCM, which will substantially enhance the C$_2$ selectivity with desired oxygen carrier recyclability.
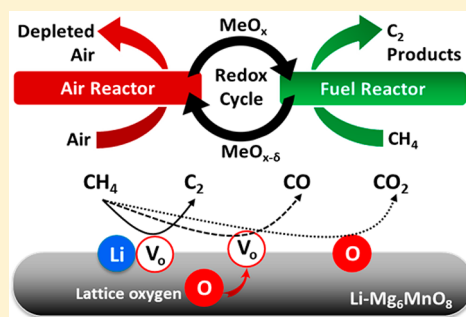
The conversion of methane to value-added chemicals has long been recognized as an important subject in energy and catalysis research concerning methane utilization.[1,2] Enormous efforts have been devoted to identifying efficient methane conversion routes and developing technologies required to accomplish them.[3,4] With the abundant supply of shale gas in recent years, industrial interest in methane conversion has intensified with even more studies conducted on this subject.[5−7] Among many possible conversion routes, oxidative coupling of methane (OCM) appears to be promising as it can convert methane to C$_2$ hydrocarbons (ethane and ethylene) in a single step.[8,9]

The typical OCM is based on the co-feed approach where methane and molecular oxygen are co-fed to a reactor containing catalyst particles.[10] It is generally understood that co-feed OCM occurs through a heterogeneous−homogeneous reaction pathway.[11] Because the desired homogeneous gas-phase reactions compete with heterogeneous reactions associated with the formation of thermodynamically stable products such as CO and CO$_2$, hydrocarbon selectivity and methane conversion follow an inversely proportional relation-

ship. The key parameter that affects this relationship in co-feed OCM is the partial pressure of gaseous oxygen.[12] Several microkinetic models for co-feed OCM indicate a greater dependence of oxygen partial pressure for producing CO/CO$_2$ than that for producing C$_2$ hydrocarbons.[13,14]

Unlike the co-feed OCM using molecular oxygen as an oxidant, chemical looping oxidative coupling of methane (CLOCM) utilizes only lattice oxygen of oxygen carriers as the oxygen source.[15,16] In CLOCM, the oxygen carrier is circulated between a fuel reactor and an air reactor. Methane is directly converted to C$_2$ hydrocarbons with oxygen carrier reduction. The reduced oxygen carriers can be regenerated by air to complete a full cycle of the redox reaction.[17,18] This process has several advantages over the co-feed approach. The major advantages of CLOCM are the elimination of a capital- and energy-intensive air separation step and no direct contact between methane and molecular oxygen, thereby avoiding the
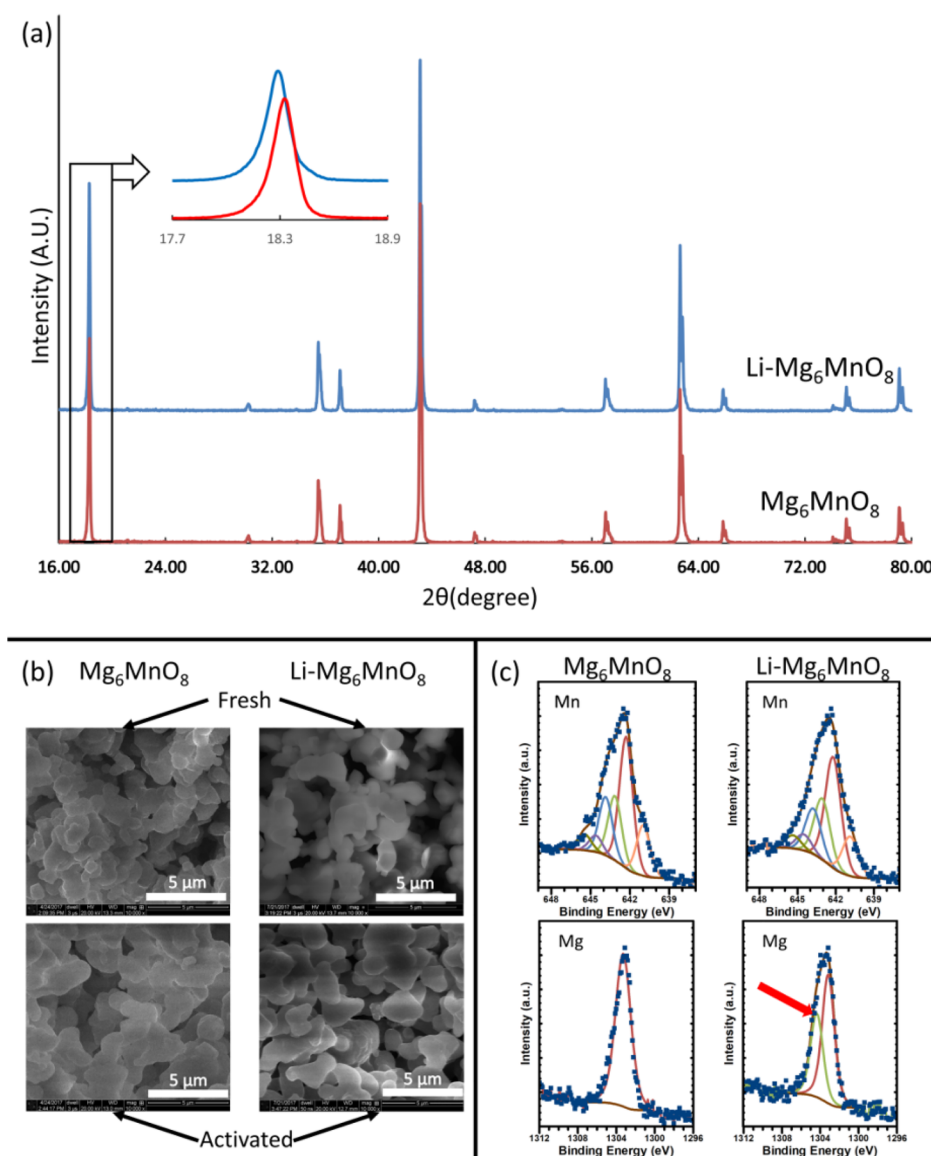
Figure 1. (a) XRD spectra for Mg_6MnO_8 and $Li-Mg_6MnO_8$; inset: high-resolution spectra of the peak corresponding to the (111) plane. (b) SEM images for fresh and activated Mg_6MnO_8 and $Li-Mg_6MnO_8$. "Fresh" sample refers to the oxygen carrier that is obtained right after calcination, and "activated" sample refers to the oxygen carrier that has undergone several redox reactions reaching steady performance. (c) XPS spectra for $Mn(2p_{3/2})$ and $Mg(1s)$ for Mg_6MnO_8 and $Li-Mg_6MnO_8$.

risk of a potentially explosive methane−oxygen mixture.[19] The major challenge for this approach is the requirement of the oxygen carriers to possess properties of high oxygen carrying, recyclability, and C_2 selectivity. Extensive efforts have been spent over the past decades on selection of a suitable oxygen carrier that can achieve high C_2 selectivity.[20−24] However, the CLOCM mechanism and the factors affecting the selectivity of oxygen carriers remain unclear.[25] New insights into the oxygen vacancy effect on methane conversion to C_2 hydrocarbon are needed, particularly in light of recent studies on methane partial oxidation that showed that the oxygen vacancy could improve methane activation in the absence of molecular oxygen.[26,27]

In recent times, novel OCM catalysts have been developed and studied on the basis of the kinetics of C_2 production pathways and catalyst composition optimization. Hedrzak and Michorczyk designed a $Mn-Na_2WO_4$ catalyst using acrylic templates coupled with different methods of loading the active

phases.[28] Hou et al. examined La-based oxides and developed a $La_2O_2CO_3$ catalyst via a hydrothermal and precipitation method with different morphologies.[29] Elkins et al. investigated rare-earth oxides for OCM and found that $Li-TbO_x/MgO$ can achieve high C_2 selectivity at temperatures above 600 °C, but its activity was not sustained.[30] Compared with these catalysts for co-feed OCM, a $Mg-Mn$ composite oxygen carrier, Mg_6MnO_8, is suitable for CLOCM due to the stable reactivity during multiple redox cycles and the high oxygen release capacity.[31]

This study investigated the enhanced C_2 selectivity of Mg_6MnO_8 in CLOCM using a low concentration (∼1%) of Li dopant. A higher concentration of Li dopant may modify the crystal phases, leading to a decrease in the oxygen carrying capacity of the carrier.[32] Li was selected as the dopant because of its high catalytic function in OCM and its similar ionic radii to Mg.[33] An enhancement mechanism was proposed and demonstrated by redox experiments and density functional
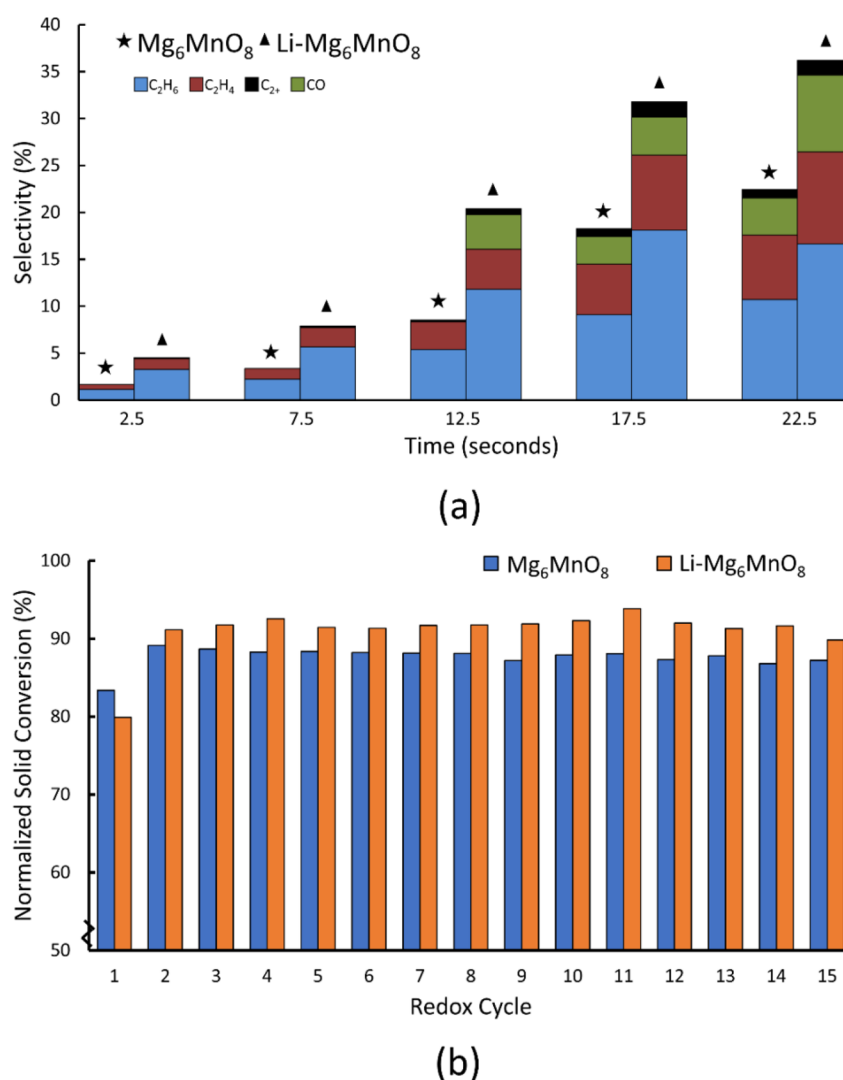
Figure 2. (a) Selectivity of hydrocarbon products (C_2H_6, C_2H_4, C_{2+}) and the partial oxidation product (CO) with reduction time over Mg_6MnO_8 and Li−Mg_6MnO_8 oxygen carriers at 850 °C. Gas samples were taken at 5 s intervals, and the gas composition was plotted against the average sample time. (b) Normalized solid conversion profiles of Mg_6MnO_8 and Li−Mg_6MnO_8 over 15 redox cycles at 850 °C.

theory calculations. It reveals how the doping-induced oxygen vacancy affects the selectivity of the oxygen carrier, thereby providing a dopant-screening strategy with the aim of facilitating systematic design of high-performance catalytic oxygen carrier for CLOCM.

Mg_6MnO_8 has a cubic murdochite-type structure that is derived from the rock-salt structure of MgO by replacement of 1/8 of the Mg^{2+} ions with Mn^{4+} ions and another 1/8 with vacancies. the XRD image in Figure 1a indicates that the undoped Mg_6MnO_8 sample can be identified as a pure Mg_6MnO_8 phase. There is a blue shift in peaks in the XRD spectra of Li-doped Mg_6MnO_8 (Li−Mg_6MnO_8), which demonstrates the incorporation of Li in the Mg_6MnO_8 lattice. SEM suggests a uniform grain size distribution in both undoped and doped samples, with an average grain size of 1 and 2 μm in freshly prepared Mg_6MnO_8 and Li−Mg_6MnO_8, respectively, as shown in Figure 1b. The grain size slightly increased to 3 and 4 μm after redox reactions, which reflects grain boundary migration and solid-state diffusion. The XPS results from Figure 1c show the spectra for $Mn(2p_{3/2})$ and Mg(1s). These spectra have been calibrated with respect to adventitious carbon at a binding energy of 284.8 eV. The

$Mn(2p_{3/2})$ spectra for both the undoped and the doped samples show multiplet splitting corresponding to the +4 oxidation state of Mn.[34] The Mg(1s) spectra, on the other hand, has an additional component in the Li−Mg_6MnO_8 sample as compared to that in the undoped Mg_6MnO_8 sample, which is shown by an arrow in Figure 1c. This additional component is seen at a binding energy of 1304.4 eV as compared to 1303.2 eV for the undoped Mg(1s) spectra. The reason for the shift to higher binding energy is mostly attributed to the Li-doping-induced electron holes being filled, thus forming charged defects, as seen in similar systems[35,36]

The selectivity toward C_2 was examined over the 25 s reduction time in the redox fixed bed experiments, and CO_2 selectivity was the balance out of 100%. From Figure 2a, it can be seen that the C_2 selectivity of the Li-doped Mg_6MnO_8 oxygen carrier in CLOCM is universally higher than that of the undoped oxygen carrier, with a maximum improvement in selectivity of 50.4% at 22.5 s prior to the start of carbon deposition. The solid conversion profile versus redox cycles was determined by thermogravimetric analysis (TGA) for both the doped and undoped samples, as seen in Figure 2b. After an initial activation period, both Mg_6MnO_8 and Li−Mg_6MnO_8
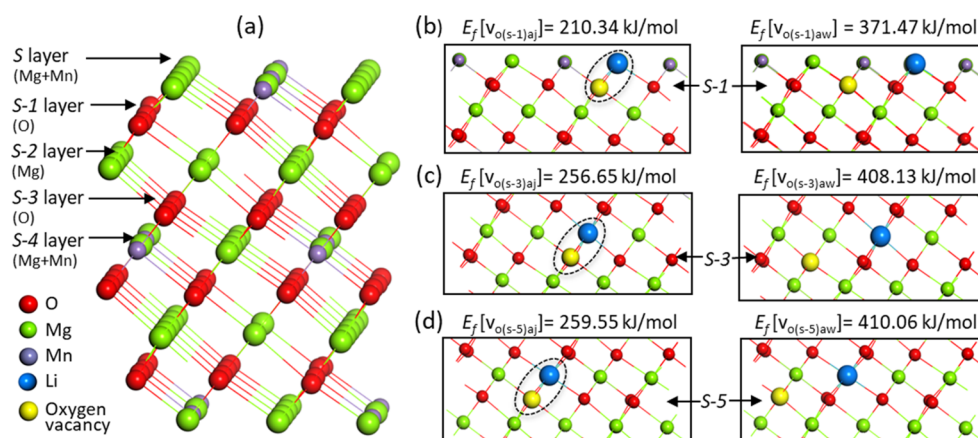
Figure 3. (a) Side view of the $Mg_6MnO_8(111)$ slab used in the calculations. The outmost layer is labeled as the s layer. Side view of the $Mg_6MnO_8(111)$ slab with the Li dopant in the s layer, s−2 layer, and s−4 layer shown in (b−d), respectively. E_f represents the oxygen vacancy formation energy where the oxygen vacancy is adjacent to the Li dopant or away from the dopant.

oxygen carrier particles give consistent reactivity across 15 redox cycles, which demonstrates good recyclability. The methane conversion profile with time is given in the Supporting Information (Figure S1). The conversion at 2.5 s is ∼90% for both the doped and the undoped samples, following the inverse relationship between selectivity and conversion.

To gain mechanistic insight into the role of the Li dopant in C_2 selectivity enhancement of the Mg_6MnO_8 oxygen carrier, first-principles calculations were performed within the framework of density functional theory (DFT) using the Vienna Ab Initio Simulation Package (VASP).[37] On the basis of surface free energy calculations, the $Mg_6MnO_8(111)$ surface was chosen as the slab model with a Mg−Mn termination, where the outermost layer was labeled as the s layer, as shown in Figure 3a. The doped system $Li_{(s)}$−Mg_6MnO_8 was built by replacing one Mg atom in the s layer with one Li atom. Because Li has a lower valence than the Mg cation, the substitution creates an electron deficit in the system that results in Mg−O bond weakening. To test whether the doping has an intriguing consequence in oxygen vacancy formation in the $Li_{(s)}$−Mg_6MnO_8 system, the formation energies of oxygen vacancies (E_f) at different positions were calculated. Two types of oxygen vacancies were considered: one adjacent to the dopant and one away from the dopant. The former was created by removing a five-fold-coordinated lattice oxygen atom in the s−1 layer, which is directly bound to the $Li_{(s)}$ dopant. This oxygen vacancy is denoted as $Vo_{(s−1)aj}$. The latter was created by removing a five-fold-coordinated lattice oxygen in the s−1 layer, which is near the $Vo_{(s−1)aj}$ but is not bound to the $Li_{(s)}$ dopant. It is denoted as $Vo_{(s−1)aw}$. The distance between $Vo_{(s−1)aw}$ and $Li_{(s)}$ dopant is 4.58 Å. If the dopant has a long-range effect, the energy of forming an oxygen vacancy far from the dopant will be different from that of forming an oxygen vacancy on the undoped oxygen carrier. If there is a short-range effect, E_f for forming a vacancy adjacent to the dopant is not equal to the energy of forming an oxygen vacancy away from it. The calculations show that E_f values for $Vo_{(s−1)aj}$ and $Vo_{(s−1)aw}$ are 210.34 and 371.47 kJ/mol, respectively, as shown in Figure 3b. In contrast, the formation energy of the oxygen vacancy in the s−1 layer of undoped Mg_6MnO_8 is 375.33 kJ/mol. It indicates that the Li dopant has a short-range effect and affects only the lattice oxygen atoms adjacent to the dopant.

In order to further confirm the dopant effect on oxygen vacancy formation, Li doping was modeled in the subsurface of the Mg_6MnO_8 slab by replacing one Mg atom in the s−2 layer with one Li atom, $Li_{(s−2)}$. $Vo_{(s−3)aj}$ represents the oxygen vacancy adjacent to the dopant $Li_{(s−2)}$, while $Vo_{(s−3)aw}$ represents the oxygen vacancy away from the dopant $Li_{(s−2)}$, as shown in Figure 3c. The energies for forming $Vo_{(s−3)aj}$ and $Vo_{(s−3)aw}$ are 256.65 and 408.13 kJ/mol, respectively. In undoped Mg_6MnO_8, the formation energy of the oxygen vacancy in the s−3 layer is 411.03 kJ/mol, which is almost equal to the formation energy of $Vo_{(s−3)aw}$ in $Li_{(s−2)}$-doped Mg_6MnO_8. For substitution in the s−4 layer, the energy of forming $Vo_{(s−5)aj}$ is 150.51 kJ/mol lower than that of forming $Vo_{(s−5)aw}$, as depicted in Figure 3d. Therefore, the doping using low-valence dopant Li can significantly reduce the energy of removing one local lattice oxygen atom and induce the formation of an oxygen vacancy that is adjacent to the dopant.

Because the formation energy of oxygen vacancy in the s−1 layer is lower than that of the subsurface oxygen vacancy, $Li_{(s)}$−Mg_6MnO_8 with $Vo_{(s−1)aj}$ was chosen as the surface model to investigate the influence of the induced oxygen vacancy on methane adsorption and activation. It is found that CH_4 adsorption at the Li site is the most stable CH_4 adsorption configuration, with an adsorption energy of 54.03 kJ/mol. For the undoped Mg_6MnO_8 surface, the strongest CH_4 adsorption configuration resides at the surface Mg site with an adsorption energy of 61.22 kJ/mol. Therefore, Li doping has not significantly affected CH_4 adsorption. The methyl radical (CH_3) is the first intermediate during CH_4 activation and dehydrogenation. On the basis of CH_3 adsorption calculations using $Li_{(s)}$−Mg_6MnO_8 with $Vo_{(s−1)aj}$, it is found that the induced oxygen vacancy is the most favorable CH_3 adsorption site and the corresponding adsorption energy is 110.96 kJ/mol. However, CH_3 adsorption on the undoped Mg_6MnO_8 surface and on $Li_{(s)}$−Mg_6MnO_8 without $Vo_{(s−1)aj}$ is found to be nearly identically stable, with adsorption energies of 147.83 and 145.35 kJ/mol. It clearly indicates that the Li-doping-induced oxygen vacancy can destabilize the adsorbed CH_3 radicals and promote their dimerization to C_2 hydrocarbons in homogeneous gas-phase reaction.

An alternative pathway for CH_3 reaction is CH_3 dehydrogenation to the methylene radical (CH_2), which will cause a decrease in C_2 selectivity. To investigate the effect of the induced oxygen vacancy on CH_3 dehydrogenation, the energy
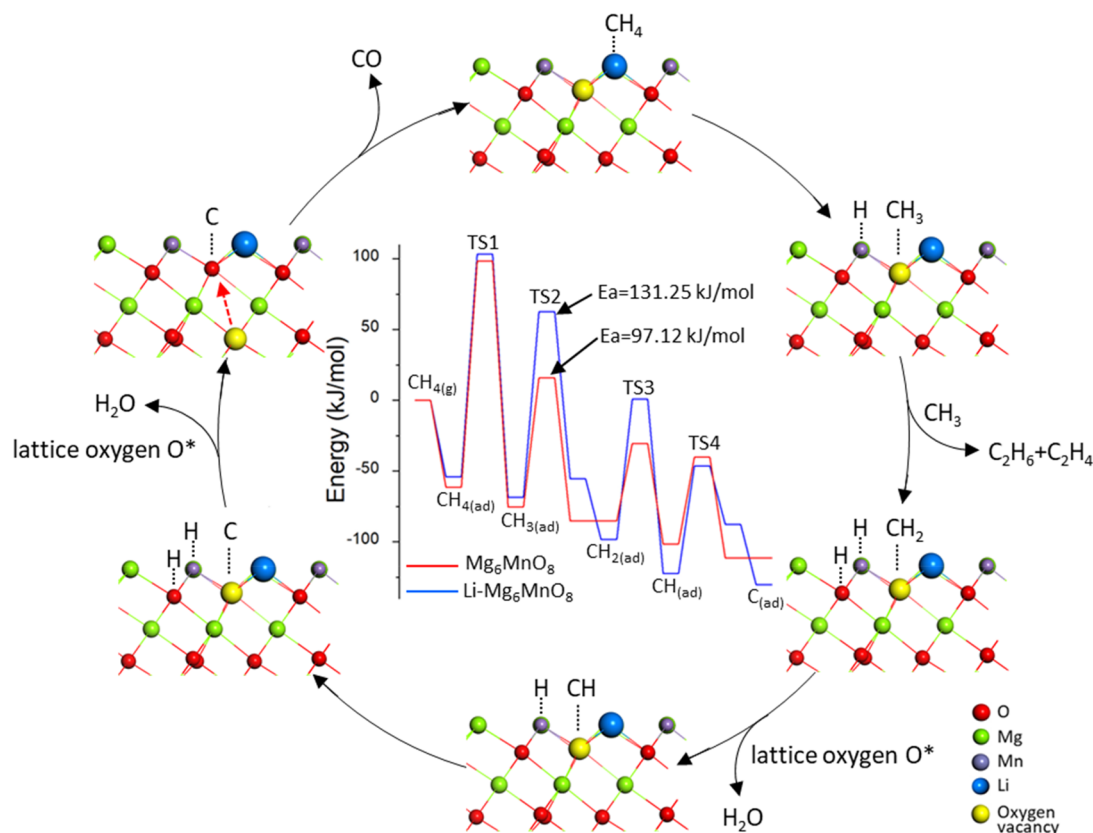
Figure 4. Proposed CH₄ activation and dehydrogenation mechanism for C₂ hydrocarbon formation on the Li−Mg₆MnO₈ oxygen carrier. The inset shows the calculated energy profiles in kJ/mol. (ad) denotes the adsorbed species, and TS denotes the transition state. The reaction cycle corresponds to the energy profile for Mg₆MnO₈ with a Li-doping-induced oxygen vacancy, which is shown by the blue line in the inset. The red line shows the energy profile for undoped Mg₆MnO₈.

profiles of the CH₄ dehydrogenation path on the undoped Mg₆MnO₈ surface and on $Li_{(s)}$−Mg₆MnO₈ with $Vo_{(s-1)aj}$ were mapped using the climbing-image nudged elastic band (CI-NEB) method,[38] as shown in Figure 4. It is observed that the CH₂ radical remains at the induced oxygen vacancy site when the extracted H migrates to the surface Mn site during CH₃ dehydrogenation on $Li_{(s)}$−Mg₆MnO₈ with $Vo_{(s-1)aj}$. The calculated energy barrier (E_a) is 131.25 kJ/mol, which is 34.13 kJ/mol higher than that of CH₃ dehydrogenation on the undoped Mg₆MnO₈. It indicates that the Li-doping-induced oxygen vacancy $Vo_{(s-1)aj}$ not only weakens the adsorption of CH₃ radicals but also inhibits their C−H bond activation. In addition, H adsorption is found to be enhanced when the extracted H atom from CH₃ moves toward the lattice oxygen in the s−1 layer. It results in the formation of OH species, which will bind another H atom to form a H₂O molecule. On the oxygen carrier surface with $Vo_{(s-1)aj}$, the CH radical also shows preferential adsorption on the induced oxygen vacancy site. The dehydrogenation of CH₂ on $Li_{(s)}$−Mg₆MnO₈ with $Vo_{(s-1)aj}$ needs to overcome an activation barrier of 97.43 kJ/mol, which is 42.85 kJ/mol higher than that on the undoped Mg₆MnO₈ surface. Similarly, it is found that the activation barrier of hydrogen abstraction from CH on $Li_{(s)}$−Mg₆MnO₈ with $Vo_{(s-1)aj}$ is 76.01 kJ/mol, which is 14.69 kJ/mol higher than that on the undoped Mg₆MnO₈ surface. It demonstrates that the Li-doping-induced oxygen vacancy also inhibits the activation of CH₂ and CH radicals. This is because the local charge transfer between the adjacent oxygen vacancy and the Li dopant annihilates the O_{2p} hole states, thereby lowering the

activity of the oxygen vacancy for CH₃ adsorption and activation. In contrast, the energy barrier of CH₃ dehydrogenation via the oxygen vacancy $Vo_{(s-1)aw}$ is 76.22 kJ/mol, which is lower than that on the undoped surface (97.12 kJ/mol). It indicates that the oxygen vacancy away from the dopant is favorable for CH₃ full dehydrogenation and CO formation because it can reduce the activation barrier of CH₃.[39] A recent study found that the addition of copper dopant to iron-based oxygen carriers could improve the chemical looping partial oxidation for CO production and affect the formation energies of oxygen vacancies, even vacancies not close to the dopant.[40] It agrees with the findings obtained in this study in which an adjacent oxygen vacancy is favorable for the formation of C₂ hydrocarbons while the oxygen vacancy away from the dopant favors the CO formation path. Thus, the Li dopant having only a short-range effect on the oxygen vacancy formation can serve as an efficient dopant for C₂ selectivity enhancement in CLOCM, which has been substantiated by the experimental test shown in Figure 2a.

In summary, a low concentration of lithium dopant can dramatically enhance the C₂ selectivity of a Mg−Mn composite oxygen carrier in CLOCM while maintaining the recyclability of the oxygen carrier. The redox experiments show that the C₂ selectivity of Mg₆MnO₈ with ∼1% Li dopant achieves an enhancement of 50.4% compared to the undoped Mg₆MnO₈ at 850 °C in the absence of molecular oxygen before the carbon deposition starts. DFT simulations are performed to systematically examine the active sites of Li-doped Mg₆MnO₈ for CH$_x$ radical adsorption and dehydrogenation. It is found the Li

dopant can facilitate the formation of one adjacent oxygen vacancy. The Li-doping-induced oxygen vacancy not only reduces the adsorption energy of the CH_3 radical but also increases the activation barrier of CH_x radicals, leading to C_2 selectivity enhancement of the $Li-Mg_6MnO_8$ oxygen carrier. It indicates that an ideal dopant for the oxygen carrier of CLOCM should have a short-range effect on the oxygen vacancy formation. On the basis of activation energy calculations, a catalytic cycle for CLOCM over the $Li-Mg_6MnO_8$ oxygen carrier is proposed where hydrogen abstraction occurs near the induced oxygen vacancy. The newly proposed cycle differs significantly from the existing Ito−Lunsford mechanism for co-feed OCM that involves chemisorbed molecular oxygen and dissociative adsorbed oxygen. This study reveals the relationship between the dopant-induced oxygen vacancy and C_2 selectivity of the oxygen carrier and provides a catalytic dopant screening strategy for C_2 selectivity enhancement in CLOCM. These findings will contribute to the systematic design of a high-performance catalytic oxygen carrier for direct methane conversion to C_2 hydrocarbons.

ASSOCIATED CONTENT

Supporting Information
The Supporting Information is available free of charge on the ACS Publications website at DOI: 10.1021/acsenergylett.8b00851.

Details of the oxygen carrier synthesis, characterization, fixed bed experiments, TGA experiments, and DFT calculations (PDF)

AUTHOR INFORMATION

Corresponding Author
*E-mail: fan.1@osu.edu.

ORCID
Zhuo Cheng: 0000-0001-7910-4264
Jonathan A. Fan: 0000-0001-9816-9979
Liang-Shih Fan: 0000-0002-2075-6505

Author Contributions
§Z.C. and D.S.B. contributed equally to this work.

Notes
The authors declare no competing financial interest.

REFERENCES

(1) Fan, L.-S. *Chemical Looping Partial Oxidation: Gasification, Reforming, and Chemical Syntheses*; Cambridge University Press: Cambridge, U.K., 2017.
(2) Holmen, A. Direct Conversion of Methane to Fuels and Chemicals. *Catal. Today* 2009, 142, 2−8.
(3) Fan, L.-S. *Chemical Looping Systems for Fossil Energy Conversions*; Wiley-AIChE: Hoboken, NJ, 2010.
(4) Olivos-Suarez, A. I.; Szécsényi, A.; Hensen, E. J. M.; Ruiz-Martinez, J.; Pidko, E. A.; Gascon, J. Strategies for the Direct Valorization of Methane Using Heterogeneous Catalysis: Challenges and Opportunities. *ACS Catal.* 2016, 6, 2965−2981.
(5) Armor, J. N. Emerging Importance of Shale Gas to Both the Energy & Chemicals Landscape. *J. Energy Chem.* 2013, 22, 21−26.
(6) Luo, S.; Zeng, L.; Xu, D.; Kathe, M.; Chung, E.; Deshpande, N.; Qin, L.; Majumder, A.; Hsieh, T.-L.; Tong, A.; Sun, Z.; Fan, L.-S. Shale Gas-to-Syngas Chemical Looping Process for Stable Shale Gas Conversion to High Purity Syngas with a H_2: CO Ratio of 2:1. *Energy Environ. Sci.* 2014, 7, 4104−4117.
(7) Kim, J.; Abbott, M. S.; Go, D. B.; Hicks, J. C. Enhancing C−H Bond Activation of Methane via Temperature-Controlled, Catalyst−Plasma Interactions. *ACS Energy Lett.* 2016, 1, 94−99.
(8) Zavyalova, U.; Holena, M.; Schlögl, R.; Baerns, M. Statistical Analysis of Past Catalytic Data on Oxidative Methane Coupling for New Insights into the Composition of High-Performance Catalysts. *ChemCatChem* 2011, 3, 1935−1947.
(9) Galadima, A.; Muraza, O. Revisiting the Oxidative Coupling of Methane to Ethylene in the Golden Period of Shale Gas: A review. *J. Ind. Eng. Chem.* 2016, 37, 1−13.
(10) Lunsford, J. H. Catalytic Conversion of Methane to More Useful Chemicals and Fuels: a Challenge for the 21st Century. *Catal. Today* 2000, 63, 165−174.
(11) Lomonosov, V. I.; Sinev, M. Yu. Oxidative Coupling of Methane: Mechanism and Kinetics. *Kinet. Catal.* 2016, 57, 647−676.
(12) Albrecht, M.; Rodemerck, U.; Linke, D.; Kondratenko, E. V. Oxidative Coupling of Methane at Elevated Pressures: Reactor Concept and Its Validation. *React. Chem. Eng.* 2018, 3, 151−154.
(13) Stansch, Z.; Mleczko, L.; Baerns, M. Comprehensive Kinetics of Oxidative Coupling of Methane over the La_2O_3/CaO Catalyst. *Ind. Eng. Chem. Res.* 1997, 36, 2568−2579.
(14) Tiemersma, T. P.; Tuinier, M. J.; Gallucci, F.; Kuipers, J. A. M.; van Sint Annaland, M. A Kinetics Study for The Oxidative Coupling of Methane on a $Mn/Na_2WO_4/SiO_2$ Catalyst. *Appl. Catal., A* 2012, 433-434, 96−108.
(15) Li, F.; Kim, R.; Sridhar, D.; Wang, F.; Zeng, L.; Chen, J.; Fan, L.-S. Syngas Chemical Looping Gasification Process: Oxygen Carrier Particle Selection and Performance. *Energy Fuels* 2009, 23, 4182−4189.
(16) Qin, L.; Cheng, Z.; Guo, M.; Fan, J. A.; Fan, L.-S.; Xu, M. Impact of 1% Lanthanum Dopant on Carbonaceous Fuel Redox Reactions with an Iron-Based Oxygen Carrier in Chemical Looping Processes. *ACS Energy Lett.* 2017, 2, 70−74.
(17) Qin, L.; Cheng, Z.; Fan, J. A.; Kopechek, D.; Xu, D.; Deshpande, N.; Fan, L.-S. Nanostructure Formation Mechanism and Ion Diffusion in Iron−Titanium Composite Materials with Chemical Looping Redox Reactions. *J. Mater. Chem. A* 2015, 3, 11302−11312.
(18) Imtiaz, Q.; Kurlov, A.; Rupp, J. L. M.; Muller, C. R. Highly Efficient Oxygen-Storage Material with Intrinsic Coke Resistance for Chemical Looping Combustion-Based CO_2 Capture. *ChemSusChem* 2015, 8, 2055−2065.
(19) Neal, L.; Shafiefarhood, A.; Li, F. Dynamic Methane Partial Oxidation Using a $Fe_2O_3@La_{0.8}Sr_{0.2}FeO_{3-d}$ Core-Shell Redox Catalyst in Absence of Gaseous Oxygen. *ACS Catal.* 2014, 4, 3560−3569.
(20) Bayanak, M.; Azimi, A. Investigation of Activity and Selectivity of Redox Catalysts in Oxidative Coupling of Methane in Fluidized Bed Reactor. *J. Fundam. Appl. Sci.* 2016, 8, 397−419.
(21) Parishan, S.; Littlewood, P.; Arinchtein, A.; Fleischer, A.; Schomäcker, R. Chemical Looping as a Reactor Concept for the Oxidative Coupling of Methane over the Mn_xO_y-Na_2WO_4/SiO_2 Catalyst, Benefits and Limitation. *Catal. Today* 2018, 311, 40−47.
(22) Greish, A. A.; Glukhov, L. M.; Finashina, E. D.; Kustov, L. M.; Sung, J.; Choo, K.; Kim, T. Oxidative Coupling of Methane in the Redox Cyclic Mode over the Catalysts on the Basis of CeO_2 and La_2O_3. *Mendeleev Commun.* 2010, 20, 28−30.
(23) Nagy, A. J.; Mestl, G.; Schlögl, R. The Role of Subsurface Oxygen in the Silver-Catalyzed, Oxidative Coupling of Methane. *J. Catal.* 1999, 188, 58−68.
(24) Sung, J. S.; Choo, K. Y.; Kim, T. H.; Greish, A.; Glukhov, L.; Finashina, E.; Kustov, L. Peculiarities of Oxidative Coupling of Methane in Redox Cyclic Mode over Ag-La_2O_3/SiO_2 Catalysts. *Appl. Catal., A* 2010, 380, 28−32.

(25) Fleischer, V.; Simon, U.; Parishan, S.; Colmenares, M. G.; Görke, O.; Gurlo, A.; Riedel, W.; Thum, L.; Schmidt, J.; Risse, T.; et al. Investigation of the Role of the Na$_2$WO$_4$/Mn/SiO$_2$ Catalyst Composition in the Oxidative Coupling of Methane by Chemical Looping Experiments. *J. Catal.* **2018**, *360*, 102−117.

(26) Cheng, Z.; Qin, L.; Guo, M.; Fan, J. A.; Xu, D.; Fan, L.-S. Methane Adsorption and Dissociation on Iron Oxide Oxygen Carrier: Role of Oxygen Vacancy. *Phys. Chem. Chem. Phys.* **2016**, *18*, 16423−16435.

(27) Cheng, Z.; Lo, C. Effect of Support Structure and Composition on the Catalytic Activity of Pt Nanoclusters for Methane Dehydrogenation. *Ind. Eng. Chem. Res.* **2013**, *52*, 15447−15454.

(28) Hedrzak, E.; Michorczyk, P. The Application of 3D Printing in the Designing of Channel Structures in Monolithic Catalysts Dedicated to the Oxidative Coupling of Methane. *Technol. Trans.* **2017**, *3*, 31−40.

(29) Hou, Y.; Han, W.; Xia, W.; Wan, H. Structure Sensitivity of La$_2$O$_2$CO$_3$ Catalysts in the Oxidative Coupling of Methane. *ACS Catal.* **2015**, *5*, 1663−1674.

(30) Elkins, T. W.; Roberts, S. J.; Hagelin-Weaver, H. E. Effects of Alkali and Alkaline-Earth Metal Dopants on Magnesium Oxide Supported Rare-Earth Oxide Catalysts in the Oxidative Coupling of Methane. *Appl. Catal., A* **2016**, *528*, 175−190.

(31) Chung, E.; Wang, W.; Nadgouda, S. G.; Baser, D. S.; Sofranko, J. A.; Fan, L.-S. Catalytic Oxygen Carriers and Process Systems for Oxidative Coupling of Methane Using the Chemical Looping Technology. *Ind. Eng. Chem. Res.* **2016**, *55*, 12750−12764.

(32) Qin, L.; Guo, M.; Cheng, Z.; Xu, M.; Liu, Y.; Xu, D.; Fan, J. A.; Fan, L.-S. Improved Cyclic Redox Reactivity of Lanthanum Modified Iron-Based Oxygen Carriers in Carbon Monoxide Chemical Looping Combustion. *J. Mater. Chem. A* **2017**, *5*, 20153−20160.

(33) Ito, T.; Lunsford, J. H. Synthesis of Ethylene and Ethane by Partial Oxidation of Methane over Lithium-doped Magnesium Oxide. *Nature* **1985**, *314*, 721−722.

(34) Biesinger, M.; Lau, L.; Gerson, A.; Smart, R. Resolving Surface Chemical States in XPS Analysis of First Row Transition Metals, Oxides and Hydroxides: Cr, Mn, Fe, Co and Ni. *Appl. Surf. Sci.* **2010**, *257*, 887−898.

(35) Richter, N. A.; Stavale, F.; Levchenko, S. V.; Nilius, N.; Freund, H.-J.; Scheffler, M. Defect Complexes in Li-doped MgO. *Phys. Rev. B: Condens. Matter Mater. Phys.* **2015**, *91*, 195305.

(36) Arndt, S.; Laugel, G.; Levchenko, S. V.; Horn, R.; Baerns, M.; Scheffler, M.; Schlögl, R.; Schomäcker, R. A Critical Assessment of Li/MgO-Based Catalysts for the Oxidative Coupling of Methane. *Catal. Rev.: Sci. Eng.* **2011**, *53*, 424−514.

(37) Kresse, G.; Furthmuller, J. Efficiency of Ab-initio Total Energy Calculations for Metals and Semiconductors Using A Plane-wave Basis Set. *Comput. Mater. Sci.* **1996**, *6*, 15.

(38) Henkelman, G.; Jónsson, H.; Uberuaga, B. P. A Climbing Image Nudged Elastic Band Method for Finding Saddle Points and Minimum Energy Paths. *J. Chem. Phys.* **2000**, *113*, 9901−9904.

(39) Cheng, Z.; Qin, L.; Guo, M.; Xu, M.; Fan, J. A.; Fan, L.-S. Oxygen Vacancy Promoted Methane Partial Oxidation over Iron Oxide Oxygen Carriers in the Chemical Looping Process. *Phys. Chem. Chem. Phys.* **2016**, *18*, 32418−32428.

(40) Qin, L.; Guo, M.; Liu, Y.; Cheng, Z.; Fan, J. A.; Fan, L.-S. Enhanced Methane Conversion in Chemical Looping Partial Oxidation Systems Using a Copper Doping Modification. *Appl. Catal., B* **2018**, *235*, 143−149.